Photoacoustic Signal Enhancement of Al- and Si-Phthalocyanines Caused by Photoinduced Cleavage of Water-Soluble Axial Ligand

Kohei Nogita, Koji Miki,* Naoto Imaizumi, Masahiro Oe, Huiying Mu, and Kouichi Ohe*

K. Nogita, Prof. K. Miki, N. Imaizumi, M. Oe, H. Mu, Prof. K. Ohe
Department of Energy and Hydrocarbon Chemistry,
Graduate School of Engineering, Kyoto University,
Katsura, Nishikyo-ku, Kyoto 615-8510, Japan
E-mail: kojimiki@scl.kyoto-u.ac.jp; ohe@scl.kyoto-u.ac.jp

Keywords: phthalocyanines, amphiphiles, self-assembly, photoacoustic, photo-responsive

Abstract

Aluminum and silicon phthalocyanines bearing water-soluble poly(ethylene glycol) as axial ligands which formed vesicles in water enhanced photoacoustic (PA) signal intensities under continuous photoirradiation. The photoinduced cleavage of axial ligands in water-soluble phthalocyanines is a key step to produce phthalocyanine aggregates which generate strong photoacoustic wave.

1. Introduction

Metallophthalocynanine (MPc), one of cyclic tetrapyrrole family, is a photostable near-infrared (NIR) dye with high molar extinction coefficient (ε) (~1.0×10^5) and low photoluminescence quantum yield (Φ) (< 0.10), converting the excited energy into strong photoacoustic (PA) wave efficiently.[1-3] Because of these properties, many researchers focused their attentions on MPcs as a promising NIR photosensitizer for practical PA imaging.[4-6] Although the reported MPc-containing PA contrast agents can generate strong PA wave, their "always-on" properties may cause the strong background signals from non-targeted tissues and blood vessels. Hence, activatable PA contrast agents based on MPcs whose PA signal intensity can be enhanced by biological stimuli have been developed.[2a,7,8] Pu and co-workers developed MPcs bearing oxidant-responsive water-soluble side chains as an activatable PA contrast agent.[9] Yoon and co-workers prepared protein-responsive MPc-based photosensitizers for tumor theranostics.[10] Toriumi, Uchiyama, and co-workers reported benziphthalocyanines which change PA signal intensities through tautomerization, as a potent activatable PA contrast agent.[11] Recently, we have developed naphthalocyanines bearing enzyme-responsive peptide and water-soluble poly(ethylene glycol) (PEG) as an axial ligand and demonstrated their application as enzyme-activatable contrast agents to *in vivo* PA tumor imaging.[12] However, the turn-on properties of these photosensitizers should be affected by the concentration of endogenous oxidant, protein, and enzyme in the target tissues. To avoid the influence of endogenous biological and chemical substances, the PA signal enhancement triggered by controllable external stimuli such as photoirradiation is ideal. In the course of our continuous investigation of MPcs bearing a water-soluble axial ligands, we found that photoirradiation induced the cleavage of axial PEG ligands in aluminum phthalocyanine (AlPc) and silicon phthalocyanine (SiPc) derivatives, resulting in the aggregation of MPcs to enhance PA signal intensity (Figure 1). Because bulky axial ligands grafted on MPcs can more efficiently suppress their aggregation compared with the peripheral decoration of MPcs, AlPc and SiPc were selected as a backbone of activatable photosensitizers. Although some of "always-on"-type water-soluble MPcs were applied to tumor therapy under photoirradiation,[14] there is no example of activatable PA probes consisting of PEG and MPcs under photoirradiation. Here, we describe the preparation of self-assemblies consisting of PEG-grafted MPc derivatives (M = Al, Si) and the evaluation

of photoactivatable enhancement of their PA signal intensity. Based on the theoretical calculation and the isolation of cleaved axial ligands, we propose that the photoinduced cleavage of axial ligands proceeds through the intermolecular electron transfer between two MPcs, followed by hydrolysis.

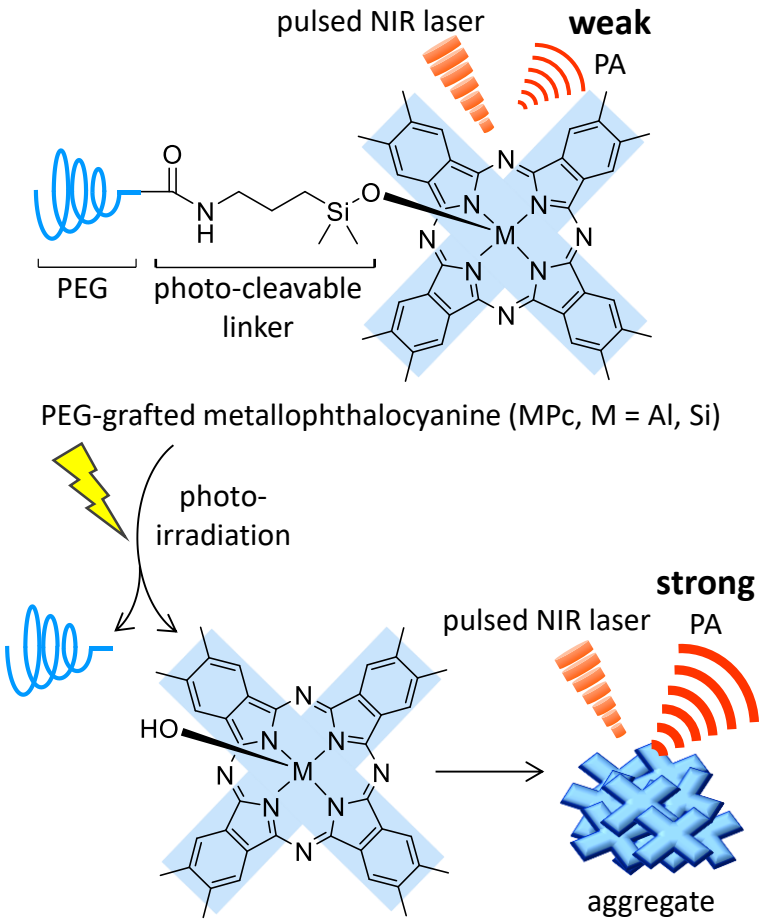

Figure 1. Photoinduced MPc aggregation for PA signal enhancement. AlPc (M = Al) and SiPc (M = Si) were used. Two PEG axial ligands were incorporated in SiPc, but one of two ligands is omitted for clarity.

2. Experimental

2.1. Materials and methods

Poly(ethylene glycol) monomethyl ether (MW = 2000) wes purchased from Sigma-Aldrich (USA). 1-Ethyl-(3-dimethylaminopropyl)carbodiimide hydrochloride (EDC·HCl) was purchased from Watanabe Chemical Industries, Ltd. (Japan). 1-Pentanol, aluminum chloride ($AlCl_3$), triethylamine, (3-aminopropyl)dimethylethoxysilane, 4-dimethylaminopyridine (DMAP), and anhydrous dichloromethane (CH_2Cl_2) were purchased from Fujifilm Wako Pure Chemicals Industries, Ltd. (Japan). 1,8-

Diazabicyclo[5.4.0]undec-7-ene (DBU), pyridine, potassium carbonate (K_2CO_3), *N*,*N*-dimethylformamide (DMF), methanol (MeOH), and succinic anhydride were purchased from Nacalai Tesque (Japan). Dichloromethane (CH_2Cl_2) and diethyl ether (Et_2O) was purchased from Kishida Chemical Co., Ltd. (Japan). Tetrachlorosilane ($SiCl_4$), quinoline, and indocyanine green (ICG) were purchased from Tokyo Chemical Industry Co., Ltd. (Japan). Dialysis membrane Spectra/Por 6 (molecular weight cutoff (MWCO): 25 kDa) was purchased from Spectrum Laboratories Inc. (Rancho Dominguez, CA, USA). Before use as a reaction solvent, pyridine and DMF were distilled over CaH_2, and MeOH was distilled over Mg. Other reagents and solvents were used as received.

UV-vis absorption spectra were recorded by UV-vis spectrophotometer (UH5300, Hitachi High Technologies, Japan).

Transmission electron microscopy (TEM, JEM-1400, JEOL Ltd., Japan) was used to visualize the morphology of dried self-assemblies. Sample solutions were dropped onto a TEM copper grid covered with a carbon film (200 mesh, Nisshin EM, Japan) and dried for 3 h before observation.

Dynamic light scattering (DLS) (FPAR-1000, Otsuka Electronics Co., Ltd., Japan) measurements were performed at scattering angles of 90° at 25 °C.

PA signals of samples in H_2O (3.0×10^{-5} M) were measured according to the reported procedure[12b] or measured by Nexus 128 (ENDRA Life Sciences Inc., USA). The sample solutions were kept in the dark at room temperature for more than 3 h before measurement. For measurement using Nexus128 apparatus, a sample solution was placed in 2 mL microtube.

Mass spectra were measured by Exactive Plus Orbitrap (ESI, Thermo Fisher Scientific Inc., USA) and Ultraflex III (MALDI, Bruker Co., USA).

2.2. Synthesis of PEGylated Pcs.

Water-soluble MPc derivatives were synthesized from metallooctamethylphthalocyanine **MPc-OH** bearing hydroxy group(s) (M = Al and Si) according to the following synthetic procedures (Scheme 1). According to the conventional phthalocyanine synthesis,[15] **MPc-OH** was prepared from phthalonitrile or diiminoisoindoline

species.

Scheme 1.

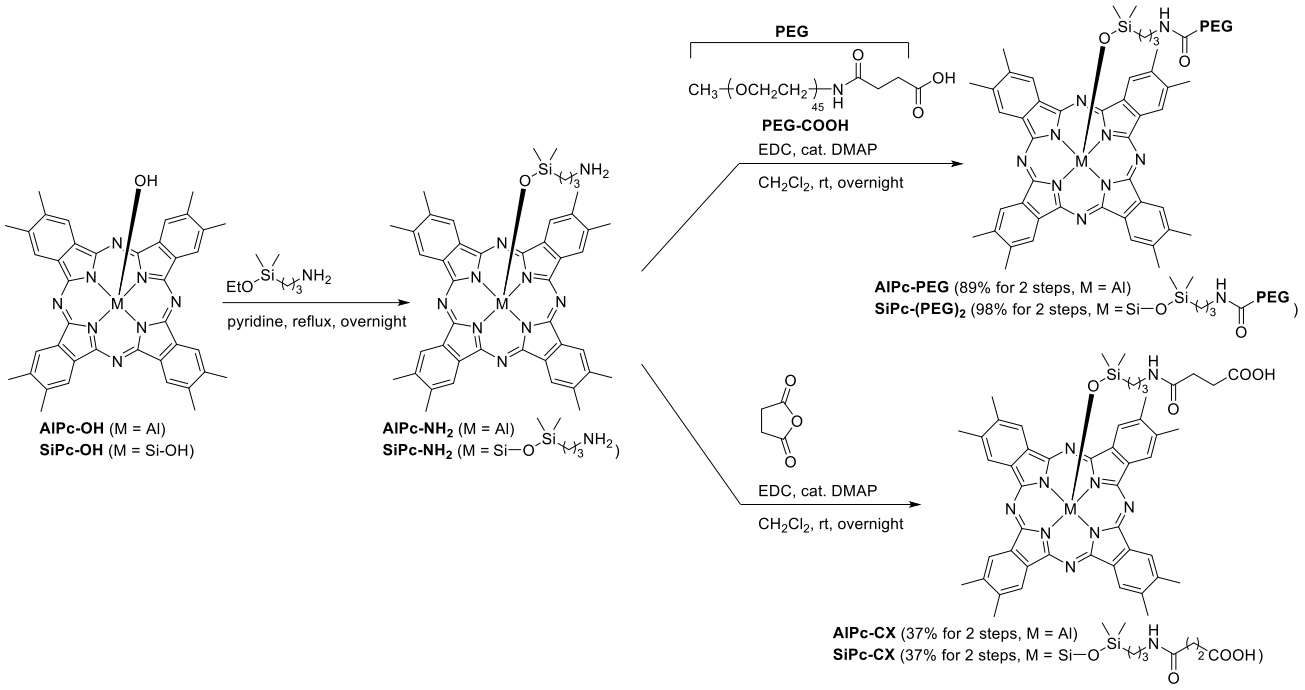

Synthesis of AlPc-OH and SiPc-OH. In a flame-dried Schlenk tube, a mixture of 4,5-dimethylphthalonitrile[16] (0.11 g, 0.67 mmol) and $AlCl_3$ (23 mg, 0.17 mmol) in 1-pentanol (1.5 mL) and DBU (0.20 mL) was stirred at 140 °C. After stirring for 23 h, the organic solvents were removed under reduced pressure. The residue was washed by MeOH (10 mL) and Et_2O (5 mL × 3), and then dried under reduced pressure to afford crude solid. A mixture of the crude solid and K_2CO_3 (0.12 g, 0.90 mmol) in H_2O (0.50 mL) and DMF (4.5 mL) was stirred at 80 °C. After stirring for 23 h, the resulting mixture was dispersed in H_2O (5.0 mL) and the blue precipitate was collected by centrifugation. The solid was washed with MeOH (10 mL) and Et_2O (5 mL × 3), and then dried under reduced pressure to afford **AlPc-OH** (60 mg, 90 μmol, 54 %) as a blue solid. No peak was observed in ^{1}H NMR spectrum because of aggregation. **AlPc-OH**: mp: >250 °C; IR (neat) 502, 508, 519, 548, 556, 579, 719, 735, 758, 813, 878, 992, 1030, 1086, 1179, 1244, 1313, 1342, 1381, 1409, 1432, 1468, 1515, 1618, 2853, 2920, 3048, 3417 cm^{-1}; HRMS (MALDI-TOF) calcd for $C_{40}H_{33}AlN_8O$ (M^+): 668.2593, found: 668.2594.

In a flame-dried Schlenk tube, a mixture of 5,6-dimethyl-1,3-diiminoisoindoline[17] (86 mg, 0.50 mmol) and

$SiCl_4$ (68 μL, 0.60 mmol) in quinoline (1.0 mL) was stirred at 200 °C. After stirring for 3.5 h, the organic solvent was removed under reduced pressure. The residue was washed by MeOH (10 mL) and Et_2O (5 mL × 3), and then dried under reduced pressure to afford crude solid (82 mg). A mixture of the crude solid (34 mg) and K_2CO_3 (29 mg, 0.20 mmol) in H_2O (0.50 mL) and DMF (4.5 mL) was stirred at 80 °C. After stirring for 23 h, the resulting mixture was dispersed with H_2O (5.0 mL) and the bluish green precipitate was collected by centrifugation. The solid was washed with MeOH (10 mL) and Et_2O (5 mL × 3), and then dried under reduced pressure to afford **SiPc-OH** (28 mg, 40 μmol, 80 %) as a bluish green solid. No peak was observed in ^{1}H NMR spectrum because of aggregation. **SiPc-OH**: mp: >250 °C; IR (neat) 503, 519, 524, 562, 584, 595, 617, 724, 738, 753, 771, 812, 880, 1020, 1040, 1082, 1135, 1180, 1206, 1315, 1345, 1378, 1411, 1433, 1471, 1520, 1619, 1657, 1738, 2938, 2971, 3046, 3455 cm^{-1}; HRMS (MALDI-TOF) calcd for $C_{40}H_{35}N_8O_2Si$ (M^+): 686.2574, found: 686.2568.

Synthesis of AlPc-NH_2 and SiPc-NH_2. Aluminum octamethylphthalocyanine **AlPc-NH_2** bearing an amino group at the end of an axial ligand was synthesized from **AlPc-OH** bearing a hydroxy group as an axial ligand according to the reported method (Scheme 1).[18] Silicon octamethylphthalocyanine **SiPc-NH_2** was synthesized from **SiPc-OH** in the similar manner.

In a 200 mL flame-dried two-necked round-bottom flask, a mixture of **AlPc-OH** (15 mg, 23 μmol) and 3-(aminopropyl)dimethylethoxysilane (50 μL, 0.20 mmol) in dry pyridine (65 mL) was stirred at 100 °C overnight under N_2 atmosphere. After stirring for 12 h, the organic solvent was removed under reduced pressure (< 40 °C). The residue was dissolved in MeOH and an insoluble solid was removed by centrifugation. After removal of solvents under reduced pressure, the residue was washed with Et_2O (5 mL × 3) and then dried under reduced pressure to afford **AlPc-NH_2** (12 mg, 14 μmol, 36%) as a blue solid. No peak was observed in ^{1}H NMR spectrum because of aggregation. **AlPc-NH_2** was used for the next reaction without further purification. **SiPc-NH_2** (~42% yield, bluish green solid) was prepared according to the similar synthetic procedure from **SiPc-OH**. 3-(Aminopropyl)dimethylethoxysilane (20 equiv) was used. The crude **SiPc-NH_2** was used in the next step without purification. **SiPc-NH_2**: ^{1}H NMR (400 MHz, $CDCl_3$, 25 °C): δ = 9.40 (s, 8H), 2.94 (s, 24H), 1.15 (t, *J* = 7.3 Hz, 4H), −1.18 to −1.26 (m, 4H), −2.28 (t, *J* = 8.2 Hz, 4H), −2.86 (s, 12H).

Synthesis of AlPc-PEG and SiPc-(PEG)$_2$. In a 50 mL flame-dried two-necked round-bottom flask, a mixture of **PEG-COOH**[19] (70 mg, 35 μmol, average molecular weight: 2000) and EDC·HCl (9.0 mg, 44 μmol) in dry CH_2Cl_2 (5.0 mL) was stirred at room temperature for 30 min. This solution was added to a solution of DMAP (2.0 mg, 25 μmol) and **AlPc-NH$_2$** (20 mg, 23 μmol) in dry CH_2Cl_2 (5.0 mL) under N_2 atmosphere, and the resulting mixture was stirred at room temperature overnight. After removal of the solvent under reduced pressure, the residue was dissolved in pure water (10 mL) and the mixture was centrifuged. The blue supernatant was dialyzed against water (MWCO : 25 kDa) for 24 h and freeze-dried to afford **AlPc-PEG** (blue solid, 58 mg, 20 μmol, 89% (assuming as a pure material), probably containing a small amount of free **PEG-COOH**) as a blue solid. **AlPc-PEG**: mp: 51–52 °C; IR (neat) 534, 548, 585, 667, 701, 737, 759, 796, 841, 962, 1060, 1102, 1147, 1241, 1342, 1360, 1410, 1467, 1548, 1645, 2742, 2883, 3295 cm^{-1}. Although signals of the PEG fragment were observed in ^1H NMR spectrum (solvent: D_2O, $CDCl_3$ or CD_3OD), no signal of AlPc was observed because of aggregation (Figure S1a). In MALDI-TOF mass spectrum of **AlPc-PEG**, the weak parent signal was observed along with signals of PEG fragments (Figure S2a).

A mixture of **PEG-COOH** (0.14 g, 70 μmol) and EDC·HCl (20 mg, 0.10 mmol) in dry CH_2Cl_2 (10 mL) was stirred at room temperature for 30 min. This solution was added to a solution of DMAP (2.0 mg, 25 μmol) and **SiPc-NH$_2$** (20 mg, 22 μmol) in dry CH_2Cl_2 (5 mL) under nitrogen atmosphere, and the resulting mixture was stirred at room temperature overnight. After removal of the solvent under reduced pressure, the residue was dissolved in pure water (10 mL) and the mixture was centrifuged. The blue supernatant was dialyzed against water (MWCO : 25 kDa) for 24 h and freeze-dried to afford **SiPc-(PEG)$_2$** (blue solid, 0.11 g, 22 μmol, 98% (assuming as a pure material), probably containing a small amount of free **PEG-COOH**) as a bluish green solid. **SiPc-(PEG)$_2$**: a bluish green solid; mp: 50–51 °C; IR (neat) 506, 516, 521, 534, 546, 570, 584, 738, 759, 795, 841, 962, 1060, 1103, 1147, 1241, 1279, 1342, 1359, 1467, 1547, 1647, 2882, 3293 cm^{-1}. Although signals of the PEG fragment were observed in ^1H NMR spectrum (solvent: D_2O, $CDCl_3$ or CD_3OD), no signal of SiPc was observed because of aggregation (Figure S1b). In MALDI-TOF mass spectrum of **SiPc-(PEG)$_2$**, the fragment peaks of SiPc bearing one PEG axial ligand and peaks of PEG fragments were observed together with the parent peaks (Figure S2b).

Synthesis of AlPc-CX and SiPc-CX. To a mixture of succinic anhydride (12 mg, 0.12 mmol) and triethylamine (25 mg, 0.25 mmol) in dry CH_2Cl_2 (5 mL) was added **AlPc-NH₂** (13 mg, 17 μmol). After stirring for 12 h, the resulting solution was washed with water and the organic layer was dried over $MgSO_4$. After the organic solvent was removed under reduced pressure, the residue was dispersed in water (10 mL) and the blue precipitate was collected by centrifugation. The crude solid was washed with Et_2O (5.0 mL × 3), and then dried under reduced pressure to afford **AlPc-CX** (5.6 mg, 6.0 μmol, 37%) as a blue solid. **AlPc-CX**: mp: >250 °C; IR (neat) 518, 526, 531, 543, 578, 598, 610, 722, 735, 757, 794, 839, 878, 1029, 1085, 1217, 1229, 1313, 1366, 1619, 1739, 2856, 2928, 2970, 3017, 3456 cm^{-1}; HRMS (MALDI-TOF) calcd for $C_{49}H_{49}AlN_9O_4Si$ [$M+H^+$]: 884.3649, found: 884.3631.

SiPc-CX was synthesized from **SiPc-NH₂** (23 mg, 26 μmol) in a similar manner of **AlPc-CX**. Succinic anhydride (36 mg, 0.36 mmol) and triethylamine (75 mg, 0.75 mmol) were used. **SiPc-CX**: a bluish green solid (11 mg, 9.4 μmol, 37% yield); mp: >250 °C; IR (neat) 509, 515, 527, 541, 561, 578, 723, 737, 758, 773, 830, 879, 1038, 1091, 1206, 1217, 1229, 1316, 1354, 1366, 1412, 1435, 1521, 1619, 1739, 2863, 2946, 2971, 3017, 3456 cm^{-1}; ^1H NMR (400 MHz, $CDCl_3$, 25 °C): δ = 9.39 (s, 8H), 2.93 (s, 24H), 2.91 to 2.87 (m, 8H), 1.16 (t, *J* = 7.2, 4H), −1.18 to −1.26 (m, 4H), −2.28 (t, *J* = 8.2 Hz, 4H) , −2.86 (s, 12H); HRMS (ESI) calcd for $C_{58}H_{67}N_{10}O_8Si_3$ [$M–H^+$]$^-$: 1115.4457, found: 1115.4459.

2.3. Preparation of self-assemblies of MPc-PEG.

Self-assemblies of **AlPc-PEG** were prepared as follows (Figure S5).[20]

Method A: Powdered **AlPc-PEG** (1.0 mg) was dissolved in Milli-Q water (3.5 mL) under sonication (100 W, 28 kHz). The resulting solution was filtered by using syringe filter (pore size: 0.45 μm) and the filtrate (**A-AlPc**) was kept in the dark at room temperature for 3 h before measurement.

Method B: Powdered **AlPc-PEG** (1.0 mg) was dissolved in CH_2Cl_2 (2.0 mL) in a 25 mL round-bottom flask. The solvent was removed by gentle blowing of nitrogen gas to prepare **AlPc-PEG** film. To this flask, Milli-Q water (3.5 mL) was added and the resulting mixture was sonicated (100 W, 28 kHz). The resulting solution was filtered by using syringe filter (pore size: 0.45 μm) and the filtrate (**B-AlPc**) was kept in the dark

at room temperature for 3 h before measurement.

Self-assemblies **A-SiPc** and **B-SiPc** were similarly prepared from **SiPc-(PEG)$_2$**. The average particle size of self-assemblies is summarized in Table 1.

Table 1. Particle size distribution and morphology of self-assemblies composed of **MPc-PEG**.

self-assembly	method	D_{DLS} (nm)	D_{TEM} (nm)	morphology
A-AlPc	**method A**	301 ± 71	143 ± 35	aggregate
B-AlPc	**method B**	307 ± 67	312 ± 149	vesicle
A-SiPc	**method A**	221 ± 44	139 ± 27	aggregate
B-SiPc	**method B**	321 ± 61	572 ± 193	vesicle

2.4. Photoinduced cleavage of axial ligands in water-soluble AlPc and SiPc.

Photostability of AlPc-PEG and SiPc-(PEG)$_2$. Each solution of **A-AlPc**, **B-AlPc**, **A-SiPc**, or **B-SiPc** in water (0.50 mg/mL) was prepared. ICG was dissolved in Milli-Q water (2.5 μM). Each solution was transferred into a quartz cuvette and irradiated using a LED photoirradiation apparatus (CL-1501, Asahi Spectra Co., Ltd., Japan) equipped with LED head unit (CL-H1-730-9-1, λ_{max} = 737 nm, half-bandwidth = 20 nm, illuminance: 25 mW (λ = 730 nm) at the sample level). The time-dependent photobleaching and nanoparticle size change were monitored by measuring the absorbance at the maximum and DLS (Table S1 and Figures S9 and S10). The precipitate was collected by centrifugation and washed several times with Milli-Q water for MALDI-TOF mass spectrometry (Figure S11).

Photoinduced cleavage of axial ligands in water-soluble AlPc and SiPc. Aqueous solutions of **A-AlPc**, **B-AlPc**, **A-SiPc**, or **B-SiPc** (0.50 mg/mL) were prepared. Each solution was transferred into quartz cuvettes and irradiated using a LED photoirradiation apparatus (CL-1501, Asahi Spectra Co., Ltd., Japan) equipped with LED head unit (CL-H1-730-9-1, λ_{max} = 737 nm, half-bandwidth = 20 nm, illuminance: 25 mW (λ = 730 nm) at the sample level). For hypoxic conditions, nitrogen bubbling was conducted for 15 min and the cuvettes were sealed during irradiation. The precipitates were collected by centrifugation. The precipitates were dissolved in conc. H_2SO_4 and the amounts of MPc derivatives were quantified by UV-vis absorbance (Figure S14) utilizing

the linear relationship as shown in Figure S15.

The fragment generated from the axial ligand under photoirradiation of **MPc-CX** was corrected as follows. **MPc-CX** (1.0 mg) was dissolved in water (10 mL) with K_2CO_3 (2.0 mg). Part of the resulting aqueous solution in a quartz cuvette (optical path length: 10 mm) was irradiated for 2 h using a Xenon light source device (MAX-303, Asahi Spectra Co., Ltd., Japan) equipped with a visible mirror module and a rod lens (RLQL80-1, illuminance: 25 mW (λ = 680 nm) at the sample level). After photoirradiation, the precipitate formed was removed by centrifugation and ESI high-resolution mass spectra of supernatant were measured to confirm the consumption of **MPc-CX** and the generation of fragments of the axial ligand (Figure S17).

For isolation of the axial ligand fragment, in a 100 mL round-bottom flask, a mixture of **MPc-CX** (4.0 mg) and K_2CO_3 (8.0 mg) in water (40 mL) was irradiated for 24 h using the same photoirradiation apparatus. To the resulting solution was added dichloromethane (20 mL) and the organic layer was separated. After neutralization with HCl aq., the organic solution was concentrated under reduced pressure to afford a white solid. ^{1}H NMR (Figure S18) and liquid chromatography-tandem mass spectrometer (LC-MS) measurements (Figures S19 and S20) of this solid were carried out. Nexera X2 UHPLC liquid chromatograph system (LC-30AD, Shimadzu Industrial System Co., Ltd. Japan) with column (InertSustain C18 (2 μm, for SiPc-CX) or InertSustainSwift C18 (1.9 μm, for AlPc-CX), 2.1 I. D. × 150 mm, GL Sciences Inc., Japan) and PDA detector (SPD M30A) was used for LC-MS/MS measurements. The mobile phase consisted of H_2O (phase A) and acetonitrile (phase B). The gradient program was set as follows, 0–3 min, 30% B; 3–5 min, 30–50% B. The flow rate was 0.3 mL/min with a pump (LC-30AD, Shimadzu Industrial System Co., Ltd. Japan). Detection was performed on a triple quadrupole mass spectrometer (LCMS-8030, Shimadzu Industrial System Co., Ltd., Japan) with an electrospray ionization (ESI) source. The parameters of the source were set under a N_2 generator (AT 10NP5NSC). The MS was operated in the negative ionization mode with the data acquisition mode of selective ion monitoring (SIM).

3. Results and Discussion

In UV-vis absorption spectra of **AlPc-PEG** and **SiPc-(PEG)$_2$** in DMF, strong signals attributed to the Q-band

of their monomeric forms were observed at 679 nm ($\varepsilon = 2.4\times10^4$ M^{-1} cm^{-1}) and 678 nm ($\varepsilon = 8.0\times10^4$ M^{-1} cm^{-1}), respectively (Figures 2a and 2b). In the case of **AlPc-PEG**, a broadened signal around 750 nm was observed besides Q-band, which indicated that a small part of **AlPc-PEG** form aggregates even in DMF solution. In regard to UV-Vis spectra of **A-AlPc** and **A-SiPc** prepared according to **method A** shown in 2.3., the sharp absorption signals of monomeric MPc decreased and new signals which are assigned as *J*-aggregates[21] were observed at 722 nm and 733 nm, respectively (Figures 2c and 2d, blue lines). Interestingly, in UV-vis spectra of **B-AlPc** and **B-SiPc**, which were prepared according to **method B** shown in 2.3., the absorbance of *J*-aggregates decreased and monomeric signal (Q-band) increased. In transmission electron microscope (TEM) observation, whereas **A-AlPc** and **A-SiPc** formed spherical nanometer-size aggregates (Figures 2e, 2g, S6, S7a, and S7c), it was observed that **B-AlPc** and **B-SiPc** formed vesicles (Figures 2f, 2h, S7b, and S7d). From dynamic light scattering (DLS) measurement, hydrodynamic diameters of self-assemblies prepared by **methods A** and **B** were estimated to be 220–320 nm (Table 1).

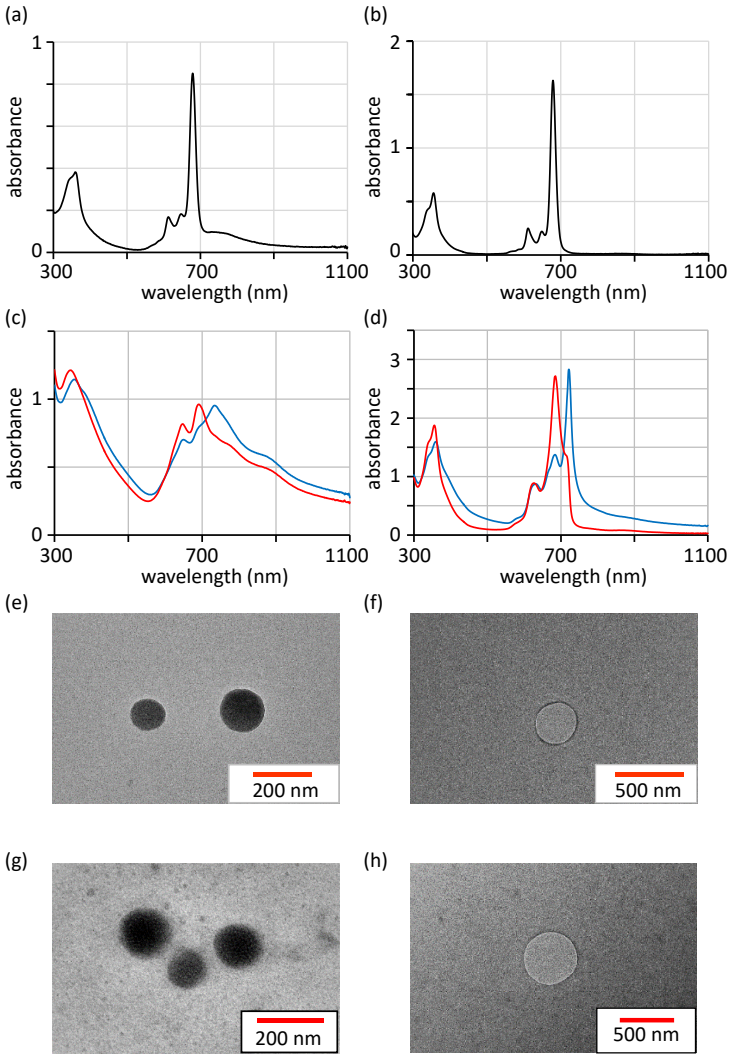

Figure 2. UV-vis absorption spectra of (a) **AlPc-PEG** (3.5×10^{-5} M) and (b) **SiPc-(PEG)$_2$** (2.0×10^{-5} M) in DMF. UV-vis absorption spectra of (c) **A-AlPc** (blue) and **B-AlPc** (red) (1.8×10^{-4} M) and (d) **A-SiPc** (blue) and **B-SiPc** (red) (1.0×10^{-4} M) in water. Representative TEM images of self-assemblies of (e) **A-AlPc**, (f) **B-AlPc**, (g) **A-SiPc** and (h) **B-SiPc**.

Crystallographic analyses of AlPcs were reported; however, their intermolecular interaction was not discussed in detail.[22] Mizuguchi and co-workers reported the titanium(IV) phthalocyanine oxide having a small axial ligand.[23] In the crystal structure, Ti(O)Pcs were packed through the concave-concave interaction (*H*-aggregation) and the convex-convex interaction (*J*-aggregation). Considering these observation and UV-vis spectra shown in Figures 2c and 2d, it was assumed that **AlPc-PEG** favors random *H*- and *J*-aggregation[24] in **A-AlPc**, whereas **B-AlPc** forms a layer of AlPc dimers with concave-concave interaction (Figure 3a). In contrast, **A-SiPc** favors *J*-aggregate forms with partial overlap of Pcs (*J*-aggregation) because of two large

hydrophilic axial ligands. The hydrophilic-hydrophobic-hydrophilic structure of **SiPc-(PEG)$_2$** facilitates forming vesicles composed of a SiPc monolayer in **B-SiPc** (Figure 3b).

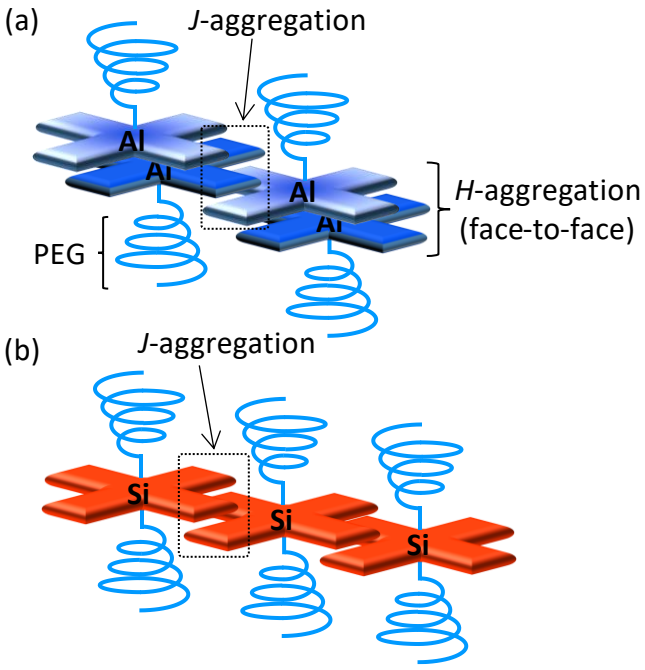

Figure 3. Plausible aggregation modes (*H*- and *J*-aggregates) in vesicles composed of (a) **B-AlPc** and (b) **B-SiPc**.

The photostability of self-assemblies was compared with indocyanine green (ICG), which is an approved NIR dye for practical diagnosis.[25] Under continuous photoirradiation using light-emitting diode (LED) at 25 mW (λ = 730 nm) for 1 h, the absorbance decrement of ICG was 45%, whereas the absorbance decrement of **A-AlPc** and **A-SiPc** were 3% and 1%, respectively (Figure 4a and Table S1). In contrast, the absorbance decrement of **B-AlPc** and **B-SiPc** were 9% and 12% for 1 h under the identical photoirradiation conditions, respectively, the precipitate being gradually generated for several hours. In MALDI-TOF mass spectra of precipitates, the parent mass numbers of **MPc-PEG** were not observed, but the corresponding fragment mass numbers of **AlPc-OH** and **SiPc-OH** were detected (Figure S11). These results indicate that the axial ligands of **AlPc-PEG** and **SiPc-(PEG)$_2$** were cleaved by continuous photoirradiation, where **MPc-OH** precipitated due to the low water solubility. Next, the PA signal intensity were monitored before/after continuous photoirradiation.[26] As expected, no change of the PA signal intensity of **A-AlPc** and **A-SiPc** was observed,

whereas PA signal intensity of vesicles **B-AlPc** and **B-SiPc** gradually increased during photoirradiation for 10–20 min and kept constant after then (Figures 4b and 4c). The DLS measurement of the irradiated solutions points out that the hydrodynamic diameters of self-assemblies of **B-AlPc** gradually increased, whereas those of **A-AlPc** showed no significant change (Figure S9). In contrast, PA signal intensities of **B-AlPc** and **B-SiPc** were not changed in the dark for 48 h (Figure S12). These results support that **AlPc-OH** generated from **B-AlPc** under photoirradiation gradually aggregated to form larger nanoparticles, enhancing PA signal intensity. It is well-accepted that the aggregation of π-conjugated dyes enhances the PA signal intensity due to fluorescence quenching.[4e,6c,27] Although Pc-based probes utilizing aggregation-induced PA signal intensity enhancement have been reported,[9] to our knowledge, this is the first example of photo-activatable PA signal intensity enhancement of MPcs.

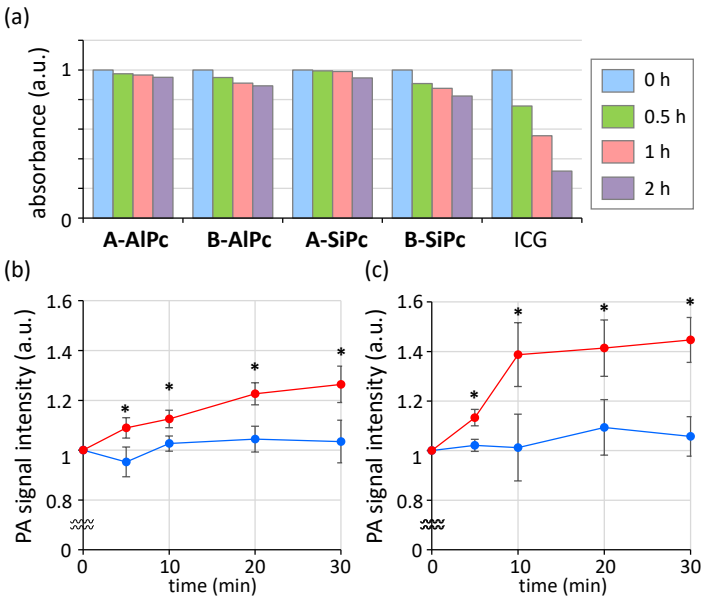

Figure 4. (a) Photostability of ICG and self-assemblies of **A-AlPc**, **B-AlPc**, **A-SiPc**, and **B-SiPc** under continuous photoirradiation at 25 mW (λ = 730 nm). Time-dependent PA signal intensity change of (b) **A-AlPc** (blue) and **B-AlPc** (red), and (c) **A-SiPc** (blue) and **B-SiPc** (red) during continuous photoirradiation at 25 mW (λ = 730 nm). PA signal intensities were measured using pulsed laser (λ_{ex} = 680 nm). Conc.: 1.0×10^{-4} M. The statistical significances were determined using a two-tailed *t*-test, $*p \leq 0.05$.

The efficiency of photoinduced cleavage of axial ligands in **MPc-PEG** was next examined by measuring UV-vis absorbance. In the case of **AlPc-PEG**, the yields of AlPc aggregates collected by centrifugation after

continuous photoirradiation were 18% (for 10 min), 32% (for 30 min), and 34% (for 60 min), respectively (Figure S14a). These results as well as time-dependent PA signal intensity change (Figures 4b and 4c) and size distribution change (Figures S9 and S10) accord to that the cleavage efficiency of axial ligand in **AlPc-PEG** was up to 30% under continuous photoirradiation for 30 min. In contrast, the yields of SiPc precipitates generated from **SiPc-(PEG)$_2$** were 6% (for 10 min), 6% (for 30 min), and 9% (for 60 min), respectively (Figure S14b). Because of the water solubility of **SiPc-PEG** bearing an unreacted PEG ligand, the yields of SiPc aggregates are much lower than those of AlPc aggregates. It is not clear that the yields of AlPc and SiPc aggregates were saturated at 30% and 10%, but it may be reasoned that the partial transformation of **MPc-PEG** leads to the morphology change from vesicles to non-photoresponsive MPc aggregates.

To clarify the mechanism for photoinduced cleavage of axial ligands, we carried out the continuous photoirradiation of their aqueous solutions of water-soluble **AlPc-CX** and **SiPc-CX** for 2 h and measured high-resolution mass spectrometry to detect photodegraded fragments of axial ligands (Figures 5a and S17). The detection of $[C_9H_{18}NO_4Si]^-$ and $[C_9H_{16}NO_3Si]^-$ ions in negative ion detection mode supports that the M-O-Si moiety of **AlPc-CX** and **SiPc-CX** was hydrolyzed. Although trialkylsilanol was not observed, the detection of siloxane **A** is sufficient evidence to support the photoinduced cleavage of axial ligands (Figures S18–S20).

Recently, Burda, Basilion, and co-workers reported that SiPc bearing $OSiMe_2(CH_2)_3NH_2$ and $OSiMe_2(CH_2)_3NMe_2$ as an axial ligand showed photoinduced decomposition.[28] Kobayashi and co-workers reported that the axial ligand $OSiMe_2(CH_2)_3N^+R_3$ in SiPc was gradually hydrolyzed by photoirradiation in the presence of one electron-donating molecules under hypoxic conditions and no cleavage occurred in the absence of one electron-donating molecules, such as sodium ascorbate and L-cysteine, or under normoxic conditions.[29] They pointed out that SiPc radical anion was generated through one electron transfer from electron-donating molecules, and then an axial ligand was cleaved by H_2O.[30] Because **MPc-PEG** undergoes the photoinduced cleavage in the absence of any external electron donors, we assumed that MPc radical anion might be generated from **MPc-PEG** through the intermolecular electron transfer between two MPc molecules or the intramolecular electron transfer from an amide moiety to an MPc core. Considering that the vesicle formation is essential for the photoinduced cleavage of axial ligands, we assumed the intermolecular electron transfer between two **MPc-**

PEGs is likely. The plausibility of the intermolecular electron transfer was supported by the density functional theory (DFT) calculation with consideration of the energy-minimized structures of the ground state, the excited state, the radical cation, and radical anion states of an MPc derivative (Figure S21). Consequently, the sum of Gibbs free energies of the ground and excited states is larger than the sum of radical cation and radical anion states (Table S2), indicating that the closely located MPcs in vesicle membrane can lead to the intermolecular electron transfer to form radical cation and radical anion pairs under photoirradiation. It has been reported that triplet MPcs (M = Al and Si) form excimers via triplet-triplet annihilation reaction and then excimers disproportionate to give MPc radical anion and MPc radical cation in protic solvents.[31] Although it is not clear whether the photoinduced electron transfer proceeds through photoredox reaction or excimer disproportionation, considering the measured redox potential of **MPc-PEG** (Table S3, Figure S22), we conclude that the generation of radical anion species through the intermolecular electron transfer is plausible pathway for the photoinduced cleavage of an axial ligand.

The plausible reaction mechanism is depicted in Figure 5b. One of MPcs in a vesicle membrane is excited by photoirradiation. One electron is transferred between closely located two MPc molecules to form a pair of radical cation and radical anion. The axial ligand as an siloxide anion from radical anion is released to generate MPc radical.[30] One electron is transferred from the MPc radical to radical cation and the resulting cation species reacts with H_2O or hydroxide to generate water insoluble **MPc-OH**. It is noted that the cleavage of axial ligands in **MPc-PEG** proceeded under both hypoxic and normoxic conditions, although the PA signal generation was slightly suppressed under normoxic conditions (Figure S23). This result also indicates that the intermolecular one electron transfer of **MPc-PEG** is less hampered by oxygen molecules. This result and high photostability of MPcs suggests that the singlet oxygen species ($^1O_2$)-mediated cleavage of an axial ligand is negligible, although MPc is known to be a photosensitizer for $^1O_2$ generation (Figure S24).[32] Because the photoirradiation efficiently enhanced the PA signal intensity in the absence of additional electron donors, MPcs having a photocleavable axial ligand in this study are one of good candidates as a photoactivatable photosensitizer in tumor theranostics.

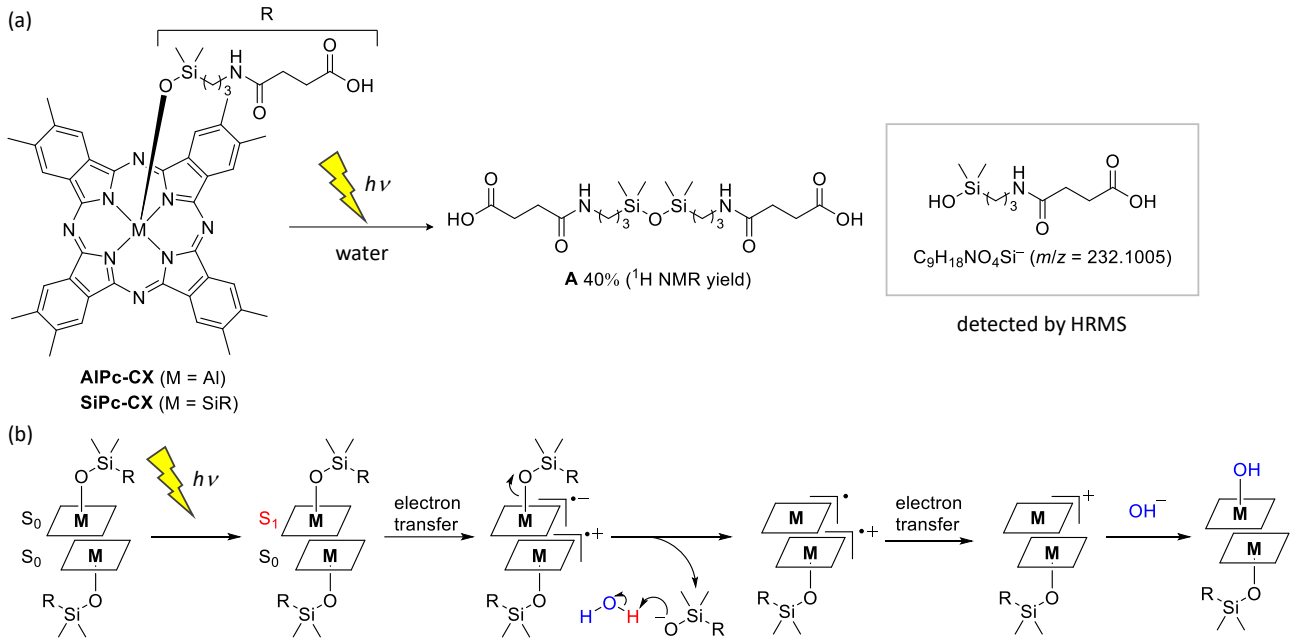

Figure 5. (a) Photoinduced cleavage of **MPc-CX**. (b) Plausible mechanism of photoinduced cleavage of axial ligands.

Conclusion

In summary, we have developed phthalocyanine derivatives **AlPc-PEG** and **SiPc-(PEG)$_2$** bearing water-soluble PEG moieties, which exhibit photoinduced enhancement of PA signal intensities via the cleavage of axial ligands. Vesicles of **MPc-PEG** prepared by **method B** gradually released axial ligand under photoirradiation to genarate water insoluble **MPc-OH**, which aggregated to form larger nanoparticles in water, enhancing their PA signal intensities up to 1.4 times. The cleavage of axial ligands in *J*-aggregates of **MPc-PEG** prepared by **method A** was not observed, resulting in no enhancement of PA signal intensity. The most plausible mechanism of the photoinduced cleavage of axial ligands involves the generation of MPc radical anion through the intermolecular one electron transfer between closely located two MPcs, followed by the hydration of radical anion. Because an amide moiety in an axial ligand is widely applicable to biological research, further modification using photocleavable axial ligand having tumor-targeting molecules will provide highly tumor-specific photoactivatable PA contrast agents in near future.

Acknowledgment

This work was supported by JSPS KAKENHI Grant Numbers 20H02811 and 21H00424. This work was supported by JST, the establishment of university fellowships towards the creation of science technology innovation, Grant Number JPMJFS2123. K.M. appreciates the financial supports from Hoansha Foundation, The Asahi Glass Foundation, Iketani Science and Technology Foundation, and the "Ishizue" project in Kyoto University. We acknowledged Prof. Teruyuki Kondo and Associate Prof. Yu Kimura in Kyoto University for PA imaging and TEM measurement.

References

[1] a) J. Weber, P. C. Beard, S. E. Bohndiek, *Nat. Methods* **2016**, *16*, 639–650. https://doi.org/10.1038/nmeth.3929 b) R. E. Borg, J. Rochford, *Photochem. Photobiol*. **2018**, *94*, 1175–1209. https://doi.org/10.1111/php.12967

[2] a) J. Huang, K. Pu, *Angew. Chem. Int. Ed*. **2020**, *59*, 11717–11731. https://doi.org/10.1002/anie.202001783 b) C. J. Reinhardt, J. Chan, *Biochemistry* **2018**, *57*, 194–199. https://doi.org/10.1021/acs.biochem.7b00888 c) H. J. Knox, J. Chan, *Acc. Chem. Res*. **2018**, *51*, 2897–2905. https://doi.org/10.1021/acs.accounts.8b00351

[3] a) X. Li, B.-D. Zheng, X.-H. Peng, S.-Z. Li, J.-W. Ying, Y. Zhao, J.-D. Huang, J. Yoon, *Coord. Chem. Rev*. **2019**, *379*, 147–160. https://doi.org/10.1016/j.ccr.2017.08.003 b) K. Mitra, M. C. T. Hartman, *Org. Biomol. Chem*. **2021**, *19*, 1168–1190. https://doi.org/10.1039/D0OB02299C

[4] a) H. Pan, S. Li, J. L. Kan, L. Gong, C. Lin, W. Liu, D. Qi, K. Wang, X. Yan, J. Jiang, *Chem. Sci*. **2019**, *10*, 8246–8252. https://doi.org/10.1039/C9SC02674F b) H.-G. Jin, W. Zhong, S. Yin, X. Zhang, Y.-H. Zhao, Y. Wang, L. Yuan, X.-B. Zhang, *ACS Appl. Mater. Inter.* **2019**, *11*, 3800–3808. https://doi.org/10.1021/acsami.8b21299 c) H. Ding, Y. Cai, J. Chen, T. Lu, W. Wen, G. Nie, X. Wang, *Microchim. Acta* **2019**, *186*, 237. https://doi.org/10.1007/s00604-019-3286-z d) R. Chen, S. Huang, T. Lin, H. Ma, W. Shan, F. Duan, J. Lv, J. Zhang, L. Ren, L. Nie, *Nat. Nanotechnol*. **2021**, *16*, 455–465. https://doi.org/10.1038/s41565-020-00844-6 e) F. Wu, L. Yue, K. Cheng, J. Chen, K.-L. Wong, W.-K. Wong, X. Zhu, *ACS Biomater. Sci. Eng*. **2020**, *6*, 5230–5239. https://doi.org/10.1021/acsbiomaterials.0c00684 f) H. D. Lu, T. L. Lim, S. Javitt, A. Heinmiller, R. K. Prud'homme, *ACS Comb. Sci*. **2017**, *19*, 397–406. https://doi.org/10.1021/acscombsci.7b00031

[5] a) D. Gao, P.-C. Lo, *J. Control. Release* **2018**, *282*, 46–61. https://doi.org/10.1016/j.jconrel.2018.04.030 b) K.

Strokov, A. H. Schäfer, U. Dobrindt, A. Galstyan, *ACS Appl. Bio Mater.* **2020**, *3*, 3751–3760. https://doi.org/10.1021/acsabm.0c00347

[6] a) S. Li, L. Zhao, R. Chang, R. Xing, X. Yan, *Chem. Eur. J.* **2019**, *25*, 13429–13435. https://doi.org/10.1002/chem.201903322 b) F. Wu, L. Chen, L. Yue, K. Wang, K. Cheng, J. Chen, X. Luo, T. Zhang, *ACS Appl. Mater. Inter*. **2019**, *11*, 21408–21416. https://doi.org/10.1021/acsami.9b06866 c) X. Li, E.-Y. Park, Y. Kang, N. Kwon, M. Yang, S. Lee, W. J. Kim, C. Kim, J. Yoon, *Angew. Chem. Int. Ed*. **2020**, *59*, 8630–8634. https://doi.org/10.1002/anie.201916147

[7] S. Xu, H.-W. Liu, S.-Y. Huan, L. Yuan, X.-B. Zhang, *Mater. Chem. Front.* **2021**, *5*, 1076–1089. https://doi.org/10.1039/D0QM00557F

[8] J. Morales, R. H. Pawle, N. Akkilic, Y. Luo, M. Xavierselvan, R. Albokhari, I. A. C. Calderon, S. Selfridge, R. Minns, L. Takiff, S. Mallidi, H. A. Clark, *ACS Sens.* **2019**, *4*, 1313–1322. https://doi.org/10.1021/acssensors.9b00209

[9] C. Xie, X. Zhen, Y. Lyu, K. Pu, *Adv. Mater*. **2017**, *29*, 1703693. https://doi.org/10.1002/adma.201703693

[10] a) X. Li, C. Kim, S. Lee, D. Lee, H.-M. Chung, G. Kim, S.-H. Heo, C. Kim, K.-S. Hong, J. Yoon, *J. Am. Chem. Soc*. **2017**, *139*, 10880–10886. https://doi.org/10.1021/jacs.7b05916 b) X. Li, S. Yu, Y. Lee, T. Guo, N. Kwon, D. Lee, S. C. Yeom, Y. Cho, G. Kim, J.-D. Huang, S. Choi, K. T. Nam, J. Yoon, *J. Am. Chem. Soc.* **2019**, *141*, 1366–1372. https://doi.org/10.1021/jacs.8b12167

[11] N. Toriumi, N. Asano, T. Ikeno, A. Muranaka, K. Hanaoka, Y. Urano, M. Uchiyama, *Angew. Chem. Int. Ed*. **2019**, *58*, 7788–7791. https://doi.org/10.1002/anie.201903303

[12] a) K. Miki, N. Imaizumi, K. Nogita, M. Oe, H. Mu, W. Huo, H. Harada, K. Ohe, *Bioconjugate Chem.* **2021**, *32*, 1773–1781. https://doi.org/10.1021/acs.bioconjchem.1c00266 b) K. Miki, N. Imaizumi, K. Nogita, M. Oe, H. Mu, W. Huo, K. Ohe, *Methods Enzymol.* **2021**, *657*, 89–109. https://doi.org/10.1016/bs.mie.2021.07.001

[13] J.-W. Hofman, F. van Zeeland, S. Turker, H. Talsma, S. A. G. Lambrechts, D. V. Sakharov, W. E. Hennink, C. F. von Nostrum, *J. Med. Chem.* **2007**, *50*, 1485–1494. https://doi.org/10.1021/jm061136w

[14] a) N. Brasseur, R. Ouellet, C. La Madeleine, J. E. van Lier, *Br. J. Cancer* **1999**, *80*, 1533–1541. https://doi.org/10.1038/sj.bjc.6690557 b) J.-J. Chen, Y.-Z. Huang, M.-R. Song, Z.-H. Zhang, J.-P. Xue,

ChemMedChem **2017**, *12*, 1504–1511. https://doi.org/10.1002/cmdc.201700384 c) K. Li, W. Dong, Q. Liu, G. Lv, M. Xie, X. Sun, L. Qiu, J. Lin, *J. Photochem. Photobiol., B* **2019**, *190*, 1–7. https://doi.org/10.1016/j.jphotobiol.2018.09.001

[15]a) J. E. Owen, M. E. Kenney, *Inorg. Chem.* **1962**, *1*, 331–333. https://doi.org/10.1021/ic50002a026 b) C. W. Dirk, T. Inabe, K. F. Schoch Jr., T. J. Marks, *J. Am. Chem. Soc.* **1983**, *105*, 1539–1550. https://doi.org/10.1021/ja00344a022

[16]J. Metz, O. Schneider, M. Hanack, *Inorg. Chem.* **1984**, *23*, 1065–1071. https://doi.org/10.1021/ic00176a014

[17]A. Weitemeyer, H. Kliesch, D. Wöhrle, *J. Org. Chem.* **1995**, *60*, 4900–4904. https://doi.org/10.1021/jo00120a038

[18]A. Galstyan, D. Block, S. Niemann, M. C. Grüner, S. Abbruzzetti, M. Oneto, C. G. Daniliuc, S. Hermann, C. Viappiani, M. Schäfers, B. Löffler, C. A. Strassert, A. Faust, *Chem. Eur. J.* **2016**, *22*, 5243–5252. https://doi.org/10.1002/chem.201504935

[19]M. E. Ourailidou, P. Dockerty, M. Witte, G. J. Poelarends, F. J. Dekker, *Org. Biomol. Chem.* **2015**, *13*, 3648–3653. https://doi.org/10.1039/C4OB02502D

[20]F. Zhou, B. Feng, H. Yu, D. Wang, T. Wang, Y. Ma, S. Wang, Y. Li, *Adv. Mater.* **2019**, *31*, 1805888. https://doi.org/10.1002/adma.201805888

[21] a) T. Doane, A. Chomas, S. Srinivasan, C. Burda, *Chem. Eur. J.* **2014**, *20*, 8030–8039. https://doi.org/10.1002/chem.201304885 b) X.-F. Zhang, Q. Xi, J. Zhao, *J. Mater. Chem.* **2010**, *20*, 6726–6733. https://doi.org/10.1039/C0JM00695E

[22]K. J. Wynne, *Inorg. Chem.* **1984**, *23*, 4658–4663. https://doi.org/10.1021/ic00194a048

[23]J. Mizuguchi, G. Rihs, H. R. Karfunkel, *J. Phys. Chem.* **1995**, *99*, 16217–16227. https://doi.org/10.1021/j100044a004

[24]a) N. B. Sul'timova, P. P. Levin, A. V. Lobanov, A. M. Muzafarov, *High Ener. Chem.* **2013**, *47*, 98–102. https://doi.org/10.1134/S0018143913030119 b) P. Juzenas, A. Juzeniene, R. Rotomskis, J. Moan, *J. Photochem. Photobiol., B* **2004**, *75*, 107–110. https://doi.org/10.1016/j.jphotobiol.2004.05.011 c) S. Dhami, D. Phillips, *J. Photochem. Photobiol., A* **1996**, *100*, 77–84. https://doi.org/10.1016/S1010-6030(96)04438-3

[25]a) T. Namikawa, J. Iwabu, M. Munekage, S. Uemura, H. Maeda, H. Kitagawa, T. Nakayama, K. Inoue, T. Sato, M. Kobayashi, K. Hanazaki, *Surg. Today* **2020**, *50*, 821–831. https://doi.org/10.1007/s00595-019-01851-4 b) C. Shi, J. B. Wu, D. Pan, *J. Biomed. Opt.* **2016**, *21*, 050901. https://doi.org/10.1117/1.JBO.21.5.050901

[26]K. Miki, T. Inoue, Y. Kobayashi, K. Nakano, H. Matsuoka, F. Yamauchi, T. Yano, K. Ohe, *Biomacromolecules* **2015**, *16*, 219–227. https://doi.org/10.1021/bm501438e

[27]a) S. Li, X. Yan, J. Zhang, X. Guo, Y. Zhang, M. Su, C. Yang, H. Zhang, C. Li, *Adv. Funct. Mater.* **2021**, 2105189. https://doi.org/10.1002/adfm.202105189 b) H. Mu, K. Miki, H. Harada, K. Tanaka, K. Nogita, K. Ohe, *ACS Sens.* **2021**, *6*, 123–129. https://doi.org/10.1021/acssensors.0c01926 c) D. Yao, S. Yang, Y. Wang, K. Bian, W. Yang, D. Wang, B. Zhang, *Nanoscale* **2019**, *11*, 6307–6314. https://doi.org/10.1039/C9NR00913B

[28]D. Luo, X. Wang, E. Walker, J. Wang, S. Springer, J. Lou, G. Ramamurthy, C. Burda, J. P. Basilion, *ACS Nano* **2020**, *14*, 15193–15203. https://doi.org/10.1021/acsnano.0c05425

[29]K. Sato, K. Ando, S. Okuyama, S. Moriguchi, T. Ogura, S. Totoki, H. Hanaoka, T. Nagaya, R. Kokawa, H. Takakura, M. Nishimura, Y. Hasegawa, P. L. Choyke, M. Ogawa, H. Kobayashi, *ACS Cent. Sci*. **2018**, *4*, 1559–1569. https://doi.org/10.1021/acscentsci.8b00565

[30]a) M. Kobayashi, M. Harada, H. Takakura, K. Ando, Y. Goto, T. Tsuneda, M. Ogawa, T. Taketsugu, *ChemPlusChem* **2020**, *85*, 1959–1963. https://doi.org/10.1002/cplu.202000338 b) E. D. Anderson, S. Sova, J. Ivanic, L. Kelly, M. J. Schnermann, *Phys. Chem. Chem. Phys.* **2018**, *20*, 19030–19036. https://doi.org/10.1039/C8CP03842B

[31]M. E. Frink, D. K. Geiger, G. J. Ferraudi, *J. Phys. Chem.* **1986**, *90*, 1924–1927. https://doi.org/10.1021/j100400a036

[32]P.-C. Lo, M. S. Rodríguez-Morgade, R. K. Pandey, D. K. P. Ng, T. Torres, F. Dumoulin, *Chem. Soc. Rev.* **2020**, *49*, 1041–1056. https://doi.org/10.1039/C9CS00129H